THE JOURNAL OF BIOLOGICAL CHEMISTRY
Vol. 280, No. 10, Issue of March 11, pp. 9074–9082, 2005
Printed in U.S.A.

Kinetics of Fibril Formation by Polyalanine Peptides*

Received for publication, June 30, 2004, and in revised form, December 10, 2004
Published, JBC Papers in Press, December 10, 2004, DOI 10.1074/jbc.M407338200

Hung D. Nguyen and Carol K. Hall‡

From the Department of Chemical and Biomolecular Engineering, North Carolina State University, Raleigh, North Carolina 27695-7905

Ordered β-sheet complexes, termed amyloid fibrils, are the underlying structural components of the intra- and extracellular fibrillar protein deposits that are associated with a variety of human diseases, including Alzheimer's, Parkinson's, and the prion diseases. In this work, we investigated the kinetics of fibril formation using our newly developed off-lattice intermediate resolution model, PRIME. The model is simple enough to allow the treatment of large multichain systems while maintaining a fairly realistic description of protein dynamics without built-in bias toward any conformation when used in conjunction with constant temperature discontinuous molecular dynamics, a fast alternative to conventional molecular dynamics. Simulations were performed on systems containing 48–96 model Ac-$KA_{14}K$-NH_2 peptides. We found that fibril formation for polyalanines incorporate features that are characteristic of three models, the templated assembly, nucleated polymerization, and nucleated conformational conversion models, but that none of them gave a completely satisfactory description of the simulation kinetics. Fibril formation was nucleation-dependent, occurring after a lag time that decreased with increasing peptide concentration and increased with increasing temperature. Fibril formation appeared to be a conformational conversion process in which small amorphous aggregates → β-sheets → ordered nucleus → subsequent rapid growth of a small stable fibril or protofilament. Fibril growth in our simulations involved both β-sheet elongation, in which the fibril grew by adding individual peptides to the end of each β-sheet, and lateral addition, in which the fibril grew by adding already formed β-sheets to its side. The initial rate of fibril formation increased with increasing concentration and decreased with increasing temperature.

Ordered β-sheet complexes are the underlying structural components of the intra- and extracellular fibrillar protein deposits, termed amyloid fibrils, that are associated with a variety of human diseases, including Alzheimer's, Parkinson's, and the prion diseases (1–6). Although extensively studied, the mechanisms that govern the formation of amyloid fibrils have not yet been fully determined. However, recent evidence that proteins other than those associated with amyloid diseases form fibrils *in vitro* under mildly denaturing conditions (7–9) has led leaders in the field to suggest that fibril formation is an intrinsic property of polypeptides, albeit under appropriate conditions. This implies that progress toward understanding the origins of various protein deposition diseases can be made by *in vitro* or *in silico* examination of the general features of protein fibrillization using model proteins that are less complex than the specific amyloidogenic protein. Here we performed computer simulations on systems containing polyalanine-based peptides of the sequence Ac-$KA_{14}K$-NH_2 in an attempt to help further understanding of the molecular level mechanisms that are responsible for fibril formation. Our molecular dynamics simulations were conducted on systems containing many peptides initially in the random-coil state.

Four mechanisms have been proposed to describe the conformational transformation and assembly of normally soluble proteins into ordered aggregates (10). The first is the templated assembly mechanism (11, 12), in which a soluble random-coil peptide binds to a preassembled β-sheet-rich nucleus and then undergoes a rate-determining structural change. The second is the monomer-directed conversion mechanism (13), in which a monomeric peptide adopts a conformation that is identical to that found in the fibril, binds to another soluble monomer in a rate-determining step, converts that monomer to the conformation found in the fibril, and then dissociates, with both peptides rapidly added to the end of the growing fibril. The third is the nucleated polymerization mechanism (14–16), which is characterized by the rate-limiting formation of a nucleus followed by the rapid addition of monomers to the growing end of the nucleus. The fourth is the nucleated-conformational conversion mechanism (17), in which the formation of small amorphous aggregates precedes the rate-limiting formation of a critical nucleus and subsequent rapid growth of large fibrils through the addition of globular multimers to fibril ends. All of the above mentioned mechanisms require that the system go through a nucleation event before fibrils can be formed. The nucleus in the monomer-directed conversion mechanism is a monomeric peptide, whereas the nuclei in the templated assembly, nucleated polymerization, and nucleated-conformational conversion mechanisms are oligomers.

The general picture of the fibril formation process that accompanies three of the four mechanisms described above, the templated assembly, nucleated polymerization, and nucleated-conformational conversion mechanisms, is the following. Fibril formation is initiated when the native state of a protein is slightly destabilized, for example, by changing pH, exposing structural elements on the resulting partially folded intermediates, which then begin to associate intermolecularly rather than intramolecularly. If the protein monomer concentration is greater than some critical concentration, the partially folded intermediates slowly associate via a series of energetically unfavorable steps, resulting in the formation of an oligomer after a defined period, called the lag time. This oligomer serves as the nucleus for the rapid growth and elongation of protofilaments or small fibrils, either through monomer addition at the

* This work was supported by grants from the National Institutes of Health (Grant GM-56766) and National Science Foundation (Grant CTS-9704044). The costs of publication of this article were defrayed in part by the payment of page charges. This article must therefore be hereby marked "*advertisement*" in accordance with 18 U.S.C. Section 1734 solely to indicate this fact.

‡ To whom correspondence should be addressed. Tel.: 919-515-3571; Fax: 919-515-3465; E-mail: hall@turbo.che.ncsu.edu.

protofilament tip or through end-to-end association of short protofilaments. Eventually, several protofilaments associate to form fibrils, which then grow further by the addition of more protofilaments. If the protein monomer concentration is less than the critical concentration, fibrillization can still take place by homogeneous (or heterogeneous) seeding in which case nucleation occurs on protein (or non-protein) species.

Most simulation studies to date of fibril-forming peptides by other investigators have been limited to the study of either isolated peptides (18–26) or model amyloid fibrils that have already formed (27–35). These studies have employed high resolution protein models, which are based on a realistic representation of protein geometry and a fairly faithful accounting for the energetics of every atom on the protein and on the solvent. Although there have been several attempts (29, 36–41) using high resolution protein models to simulate the formation of fibrils from random coils, the systems considered did not contain enough peptides to mimic the nucleus that stabilizes the large fibrils that are observed in experiments. Given current computational capabilities, simpler models are required. This has been recognized by a few investigators who have combined intermediate resolution protein models with the Go potentials to look at fibril formation. Such an approach has been taken by Jang *et al.* (42, 43), who studied the thermodynamics and kinetics of the assembly of four model β-sheet peptides into a tetrameric β-sheet complex, and by Ding *et al.* (44), who studied the formation of a fibrillar double β-sheet structure containing eight model Src SH3 domain proteins. However, since the Go potential contains a built-in bias toward the native conformation, this approach is not suitable for the study of spontaneous fibril formation from random configurations.

We developed an alternative approach, inspired in part by the models of Sun (45), Sun *et al.* (46), and Takada *et al.* (47), that represents each amino acid residue with three backbone beads and one side chain bead. Our model, which we now call PRIME (Protein Intermediate Resolution Model), allows the treatment of large multichain systems while maintaining a fairly realistic description of protein dynamics without built-in bias toward any conformation (48, 49). By combining PRIME (described below) with discontinuous molecular dynamics simulation, we have been able to simulate the formation of small fibrils or protofilaments by systems containing between 12 and 96 16-residue Ac-KA_{14}K-NH_2 peptides starting from the random-coil state. This model, which was developed by Smith and Hall (48, 50, 51) and later improved by us (49), represents each amino acid with four beads, three for the backbone and one for the side chain. It is designed to be used with discontinuous molecular dynamics (DMD)[1] (52–55), an extremely fast alternative to traditional molecular dynamics that is applicable to systems of molecules interacting via discontinuous potentials, *e.g.* hard sphere and square well potentials. Solvent is modeled implicitly by including hydrophobic interactions between nonpolar side chains. Backbone hydrogen bonding is modeled in explicit detail. The applicability of our model to polyalanine was tested in a previous study of isolated polyalanine in which we examined the predicted folding transition and the conditions under which common structures such as the α-helix and β-hairpin appear (49). Specifically, we examined the effect of temperature on the populations of the various structural states of the peptide, calculated the Zimm-Bragg equilibrium constants for propagation and nucleation of the helix, measured the hydrogen bond distances and angles for polyalanine in the α-helix and β-hairpin, and mapped out the Ramachandran plot. We found that our results agree with experimental and other simulation data very well. Although PRIME gives a fairly realistic description of polyalanine, it is essentially a work in progress; we are now in the process of extending the model to the rest of the amino acids.

By combining PRIME with DMD, we were able to sample much wider regions of conformational space, longer time scales, and larger systems than in traditional molecular dynamics (56). Since the simulations take only days on a work station, we were able to conduct simulations at a wide variety of concentrations and temperatures and to learn how peptide concentration and temperature affect the formation of various Ac-KA_{14}K-NH_2 structures, including amorphous aggregates, α-helices, β-sheets, and fibrils. All simulations were performed in the canonical ensemble starting from a random coil configuration equilibrated at a high temperature and then slowly cooled to the temperature of interest so as to minimize kinetic trapping in local free energy minima.

In this study, we investigated the kinetics of fibril formation of Ac-KA_{14}K-NH_2 peptides as a function of the peptide concentration and temperature. Simulations were conducted on systems containing 48 model 16-residue peptides at a wide variety of concentrations and temperatures using the same protein model as in our previous studies (56). All simulations were performed in the canonical ensemble; constant temperature was achieved by implementing the Andersen thermostat method (57) in which united atoms were subjected to random collisions with ghost particles, the velocities of which were chosen randomly from a Maxwell-Boltzmann distribution centered at the system temperature. During each simulation, the formation of different structures such as α-helices, aggregates, β-sheets, or fibrils was monitored as a function of time. Key fibril-forming events associated with the four proposed fibril-forming mechanisms mentioned earlier were identified. Two types of simulations were conducted: unseeded and seeded. In the unseeded simulations, the peptides, which were initially in a random coil configuration, were equilibrated at a high temperature and then quickly cooled to the temperature of interest. The lag time and rate of fibril formation were monitored to study their dependence upon the peptide concentration and temperature. In the seeded simulations, a previously created single small fibril was immersed in a sea of denatured chains.

The model peptide chosen for study is the polyalanine-based peptide Ac-KA_{14}K-NH_2. We focused on polyalanine-based peptides for three reasons. First, the small, uncharged, unbranched nature of alanine residues is amenable to simulation with the intermediate resolution protein model that we developed previously (48, 50). Second, polyalanine repeats have been implicated in human pathologies, notably in the formation of anomalous filamentous intranuclear inclusions in oculopharyngeal muscular dystrophy patients (58). Third, synthetic polyalanine-based peptides have been shown by Blondelle and co-workers (59, 60) to undergo a transition from α-helical structures to β-sheet complexes *in vitro*, mimicking the structural transition that is believed to be a prerequisite for fibril nucleation and growth (1, 61–66). Blondelle and co-workers (59, 60) observed that the α-helical structures were stabilized in part by intramolecular α-helical bonds and that the macromolecular β-sheet complexes were stabilized by hydrophobic intersheet interactions. Using circular dichroism, Fourier transform infrared spectroscopy, and reversed phase high performance liquid chromatography, they found that: 1) β-sheet complex formation increased with increasing temperature, exhibiting an S-shaped dependence on temperature with a critical temperature of 45 °C at a peptide concentration of 1.8 mM and an

[1] The abbreviations used are: DMD, discontinuous molecular dynamics; HP, hydrophobic interactions; HB, hydrogen bonds.

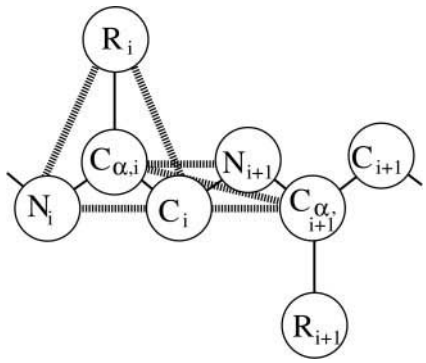

FIG. 1. **Geometry of the intermediate resolution protein model, PRIME.** Covalent bonds are shown with *narrow black lines* connecting beads. At least one of each type of pseudobond is shown with a *thick disjointed line*. Pseudobonds were used to maintain backbone bond angles, consecutive C_α distances, and residue L-isomerization. Note that the beads are not shown full size for ease of viewing.

incubation time of 3 h and 2) β-sheet complex formation increased with increasing peptide concentration above a critical concentration of 1 mM at 65 °C. Blondelle and co-workers (59, 60) did not investigate the *in vitro* kinetics of the assembly of amyloid fibril by polyalanines. This means that we could not compare our simulation data with experimental results directly. Instead we compared our results with the general features of the available kinetic models since these were formulated on the basis of experimental observations of fibril formation by other peptides.

Highlights of our results are as follows. We observed that fibril formation of polyalanines in our simulations was not perfectly described by any of the proposed fibril formation mechanisms available in the literature. It did, however, share certain features in common with three of the proposed mechanisms: templated assembly, nucleated polymerization, and nucleated conformational conversion. These common features were that: 1) fibril formation was nucleation-dependent and 2) the lag time, which is the delay time before fibril formation commences, increased with increasing temperature. As suggested by the nucleated polymerization model, the lag time at high temperatures decreased more or less exponentially as a function of the peptide concentration. As suggested by the templated assembly model, the lag time at low temperatures decreased more or less linearly with increasing peptide concentration. As predicted by the nucleated conformational conversion model, small amorphous aggregate formation preceded critical nucleus formation. Fibril growth in our simulations involved both β-sheet elongation, in which the fibril grew by adding individual peptides to the end of each β-sheet, and lateral addition, in which the fibril grew by adding already formed β-sheets to its side. The initial rate of fibril growth increased with increasing concentration and decreased with increasing temperature.

MATERIALS AND METHODS

Model Peptide and Forces—The model peptide had the sequence $PH_{14}P$, where H is a hydrophobic amino acid residue and P is a polar amino acid residue. This sequence was chosen to mimic Ac-$KA_{14}K$-NH_2 peptides, which have been shown to form stable, soluble β-sheet complexes *in vitro* (59, 60). The peptide was modeled using PRIME, an intermediate resolution model (48–51) based on a four-bead amino acid representation with realistic bond lengths and bond-angle constraints that has the ability to interact both intra- and intermolecularly via hydrogen bonding and hydrophobic interaction potentials. The geometry of the PRIME protein model is illustrated in Fig. 1. Each amino acid residue was composed of four spheres, a three-sphere backbone comprised of united atom NH, C–H, and C=O, and a single bead side chain R (labeled *N*, C_α, *C*, and *R*, respectively, in the figure). All backbone bond lengths and bond angles were fixed at their ideal values; the distance between consecutive C_α atoms was fixed so as to maintain the interpeptide bond in the trans configuration. The side chains were held in positions relative to the backbone so that all residues are L-isomers. Details of the model including values for all parameters are given in our earlier studies (48, 49).

The solvent was modeled implicitly in the sense that its effect was factored into the energy function as a potential of mean force. All forces were modeled by either hard sphere or square well potentials. The excluded volumes of the four beads were modeled using hard sphere potentials with realistic diameters. Covalent bonds were maintained between adjacent spheres along the backbone by imposing hard sphere repulsions whenever the bond lengths attempted to move outside of the range between $l(1 - \delta)$ and $l(1 + \delta)$, where l is the bond length and δ is a tolerance which we set equal to 2.375%. Ideal backbone bond angles, C_α-C_α distances, and residue L-isomerization were achieved by imposing pseudobonds, as shown in Fig. 1, which also fluctuated within a tolerance of 2.375%. Hydrogen bonding between amide hydrogen atoms and carbonyl oxygen atoms on the same or neighboring chains was represented by a square well attraction of strength ϵ_{HB} (where HB is hydrogen bonds) between NH and C=O united atoms whenever: 1) the virtual hydrogen and oxygen atoms (the location of which can be calculated at any time) were separated by 4.2 Å (the sum of the NH and C=O well widths), 2) the nitrogen-hydrogen and carbon-oxygen vectors pointed toward each other within a fairly generous tolerance, 3) neither the NH nor the C=O was already involved in a hydrogen bond with a different partner, and 4) the NH and C=O were separated by at least three intervening residues along the chain. To satisfy the second requirement, the separations between the four auxiliary pairs N_i-$C_{\alpha,j}$, N_i-N_{j+1}, C_j-$C_{\alpha,j}$, C_j-C_{i-1} surrounding the hydrogen bond in question were limited to certain distances that were chosen to maintain ideal hydrogen bond angles. This was accomplished by imposing square-shoulder interactions between the auxiliary pairs as suggested by Ding *et al.* (67). Besides adding stability to the hydrogen bond, these interactions exacted a penalty for breaking a hydrogen bond when any one of these auxiliary pairs moved inside the specified separation and thus distorted the hydrogen bond angle. For more details on the hydrogen bonding model used here, see the study by Nguyen *et al.* (49). Interactions between hydrophobic side chains were represented by a square well potential of depth ϵ_{HP} and range 1.5 σ_R, where σ_R is the side chain bead diameter and HP is hydrophobic interactions. Hydrophobic side chains had to be separated by at least three intervening residues to interact. For simplicity, the ratio of the strength of a hydrophobic contact, ϵ_{HP}, and the strength of a hydrogen bond ϵ_{HB}, $R = \epsilon_{HP}/\epsilon_{HB}$, was set equal to 1/10. Hydrogen bond strength and hydrophobic contact strength were independent of temperature, as was assumed in previous simulation studies (50, 51, 68). The rationale for including the hydrophobicity but not the hydrophilicity in our force field was that hydrophobicity is thought to be the main driving force for folding; it brings the hydrophobic side chains together and buries them in the interior. Restricting the interactions solely to hydrophobic interactions and hydrogen bonding also improved our computational efficiency, which is critical in a study of protein fibrillization.

Discontinuous Molecular Dynamics—Simulations were performed using the DMD simulation algorithm (52–55), which is an extremely fast alternative to traditional molecular dynamics and is applicable to systems of molecules interacting via discontinuous potentials, *e.g.* hard sphere and square well potentials. Unlike soft potentials such as the Lennard-Jones potential, discontinuous potentials exert forces only when particles collide, enabling the exact (as opposed to numerical) solution of the collision dynamics. DMD simulations proceed in the following fashion. The initial positions of the beads on the model protein were assigned at random but could not violate any of the size constraints or assigned bond lengths and angles. The initial velocities were chosen at random from a Maxwell-Boltzmann distribution at a fixed reduced temperature, $T^* = k_BT/\epsilon_{HB}$, where k_B is Boltzmann's constant, T is the temperature, and ϵ_{HB} is the depth of the square well hydrogen bond potential. The simulation proceeded according to the following schedule: identify the first event, move forward in time until that event occurs, calculate new velocities for the pair of beads involved in the event, and calculate any changes in system energy resulting from hydrogen bond events or hydrophobic interactions, find the second event, and so on. Types of events included excluded volume events, bond events, and square well hydrogen bond and hydrophobic interaction events. An excluded volume event occured when the surfaces of two hard spheres collided and repelled each other. A bond (or pseudobond) event occurred via a hard sphere repulsion when two adjacent spheres attempted to move outside of their bond length. Square well events included well capture, well bounce, and well dissociation collisions

when a sphere entered, attempted to leave, or left the square well of another sphere. For more details on DMD simulations with square well potentials, see studies by Alder and Wainwright (52) and Smith *et al.* (69).

Simulations were performed in the canonical ensemble, which means that the number of particles, volume, and temperature were held constant. A constant number of particles and volume was achieved by creating a virtual three-dimensional box for the simulation and allowing the model protein chains to move within that box. Periodic boundary conditions were used to eliminate artifacts due to simulation box walls. The dimensions of the box were chosen to ensure that a chain could not interact with more than one image of any other chain. For this study, we used cubic boxes with sides ranging from 200 to 430 Å in length depending on the peptide concentration. Constant temperature was achieved by implementing the Andersen thermostat method (57) as was used previously (48, 70). With this procedure, all beads in the simulation were subject to random collisions with ghost particles. The postevent velocity of a bead colliding with a ghost particle was chosen randomly from a Maxwell-Boltzmann distribution at the simulation temperature. Time was measured in terms of the reduced time t^*, which is defined as $t^* = t/\sigma(k_BT/m)^{1/2}$ with t the simulation time and σ and m the average bead diameter and mass, respectively. Since DMD simulations are collision-driven, rather than time-driven, and the solvent was modeled implicitly, it is difficult to correlate collision times with real time. Thus, when comparing our data as a function time, we used only reduced simulation time.

In the unseeded simulations, each system was started from a random coil configuration equilibrated at a high temperature, $T^* = 0.25$, and then quickly cooled down to the temperature of interest, $T^* = 0.08$, 0.09, 0.10, 0.11, 0.12, 0.13, 0.14, and 0.15. The number of ghost collisions is set at 1.0% of the total number of collisions during a simulation. The resulting cooling rate is $\Delta T^*/\Delta t^* = 0.04$ during the first 1,000,000 collisions (up to $t^* = 0.1$), after which the system temperature remains constant. Simulations are conducted on systems containing 48 peptides at concentrations c = 1, 2.5, 3.75, 5, and 10 mM. At each temperature and concentration, at least 10 simulations are conducted.

In the seeded simulations, each of the 10 systems initially contained fibrillar structures, which were obtained at the end of the 10 c = 1.0 mM and $T^* = 0.13$ unseeded 48-peptide simulations described above. Forty-eight denatured chains were added to the simulation box by randomly picking empty spaces in the simulation box and inserting the new denatured chains one by one. Each of the resulting 96-peptide systems at c = 2.0 mM was quickly heated to the temperature of interest, T^* = 0.14 and 0.15.

All systems were simulated for very long times. The simulations were stopped when the ensemble averages of the total potential energy of the system varied by no more than 2.5% over the last three quarters of the simulation run. Simulations took between 40 h at $T^* = 0.08$ and 160 h at $T^* = 0.15$ on a single processor of an AMD Athlon MP 2200+ work station.

The results presented in this study are averages from at least 10 simulations at each temperature and concentration with error bars taken from the standard deviations at each time. The structures were defined in the following way. If 12 intrapeptide α-helical hydrogen bonds (bonds between N_{i+4} and C_i) were formed, the structure was an α-helix. If each peptide in a group of peptides had at least seven interpeptide β-hydrogen bonds to a particular neighboring peptide in the group, this group was a β-sheet. If at least 2 β-sheet structures formed intersheet hydrophobic interactions (at least four hydrophobic interactions per peptide per β-sheet) and the β-sheet structures were at an angle less than 35°, this was a fibril; otherwise, this and isolated β-sheets were classified as non-fibrillar β-sheet structures. If each peptide in a group of peptides had at least two interpeptide hydrogen bonds or hydrophobic interactions with a neighboring peptide in the same group, that group was an aggregate. Aggregates that were fibrils or non-fibrillar β-sheets were amorphous aggregates. Single peptide structures that were not α-helices or β-structures were random coils.

RESULTS AND DISCUSSION

Since this study builds upon our previous work (56) on the fibril formation of peptides of the same sequence, it is useful to briefly review those results that are pertinent to the discussion here. We investigated how peptide concentration and temperature affect the formation of various Ac-KA_{14}K-NH_2 structures including α-helices, β-sheets, and fibrils. Simulations were conducted on systems of 12, 24, 48, and 96 model 16-residue peptides at a wide variety of concentrations and temperatures by applying the discontinuous molecular dynamics simulation algorithm to our intermediate resolution protein model, PRIME. All simulations were performed in the canonical ensemble starting from a random coil configuration equilibrated at a high temperature and then slowly cooled to the temperature of interest so as to minimize kinetic trapping in local free energy minima. Structural characteristics such as the peptide arrangement and packing within fibrils were examined and compared with those observed in experiments. We also studied the overall stability of fibrils by conducting simulations on already formed fibrils over a wide range of temperatures to investigate the relative importance of hydrogen bonding and hydrophobic interactions on fibril stability. The stability of our fibrillar structures was evaluated by comparing the abilities of the system to maintain the fibrillar structures at various temperatures that were higher than the fibril formation temperature.

We were able to observe the formation of small fibrils containing 12–96 polyalanine peptides starting from random coils in a relatively short period of time ranging between 40 and 160 h on a single processor of an AMD Athlon MP 2200+ work station. To our knowledge, these were the first simulations to span the whole process of fibril formation from the random coil state to the fibril state on such a large system. We found that there was a strong relationship between the formation of α-helices, β-sheets, aggregates, and fibrils and the environmental conditions such as temperature, concentration, and hydrophobic interaction strength. At low concentrations, $c < 1.0$ mM, random-coil peptides assembled into α-helices at low temperatures and random coils at high temperatures, $T^* > 0.10$. At intermediate concentrations, c = 1.0 − 2.5 mM, random-coil peptides assembled into α-helices at low temperatures, T^* = 0.08 − 0.10 and large β-sheet structures at high temperatures, $T^* = 0.11 - 0.14$. At high concentrations, $c > 2.5$ mM, random-coil peptides formed β-sheets over a wide range of temperatures, $T^* = 0.08 - 0.14$. These β-sheets assembled into fibrils above a critical temperature that decreased with concentration and exceeded the folding temperature of the isolated peptide ($T^* = 0.11$). At very high temperatures, $T^* = 0.15$, and all concentrations, the system was in a random-coil state. The critical concentration for fibril formation was between c = 1.0 mM and c = 2.5 mM at high temperatures $T^* = 0.12 - 0.14$. These results are in qualitative agreement with the experimental results of Blondelle and co-workers (59, 60) on Ac-KA_{14}K-NH_2 peptides. The fibrils observed in our simulations mimicked the structural characteristics observed in experiments in that most of the peptides in our fibrils were arranged in an in-register parallel orientation (71–73), with intrasheet and intersheet distances similar to those observed in experiments (74–76), and contained about six multipeptide β-sheets (74, 77). Finally, we found that when the strength of the hydrophobic interaction between non-polar side chains relative to the strength of the hydrogen bonds was increased from R = 1/10 to R = 1/6, the system formed amorphous rather than fibrillar aggregates. We also identified key fibril-forming events. Since simulations were conducted by slowly cooling the system down to the temperature of interest, analysis of the temperature dependence of the kinetics of fibril formation was not appropriate.

Fibril Formation Is Preceded by the Formation of Amorphous Aggregates—We found that fibril formation is a conformational conversion process in which the appearance of amorphous aggregates precedes β-sheet formation and then nucleus formation. This can be seen in Fig. 2, which shows snapshots of the fibrillization process, which were taken at various reduced times, t^*, for the 48-peptide simulation at $T^* = 0.14$ and a

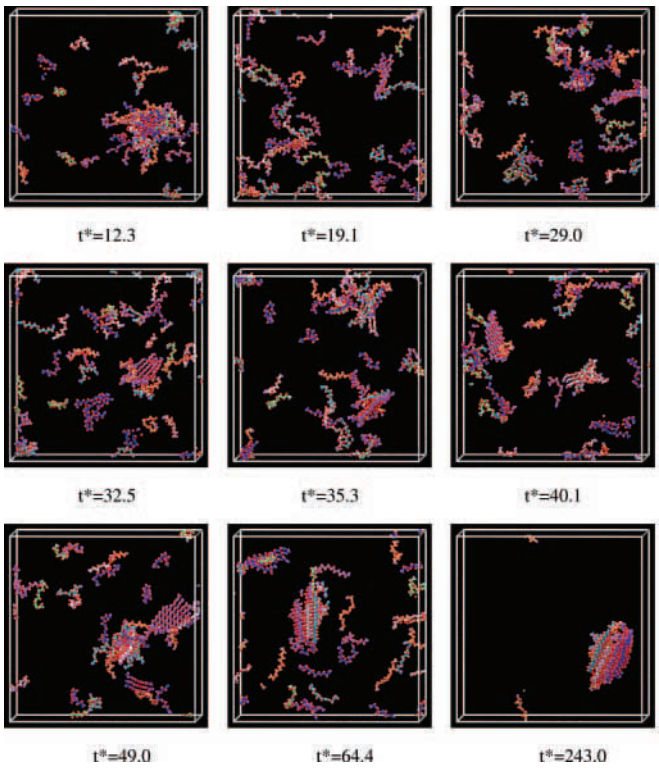

FIG. 2. **Snapshots of the 48-peptide system at various times during a simulation at c = 10 mM and T^* = 0.14 that results in the formation of a fibril.** All hydrophobic side chains are *red*; backbone atoms of different peptides have different colors, assigned so that it will be easy to distinguish the various sheets once the fibril is formed.

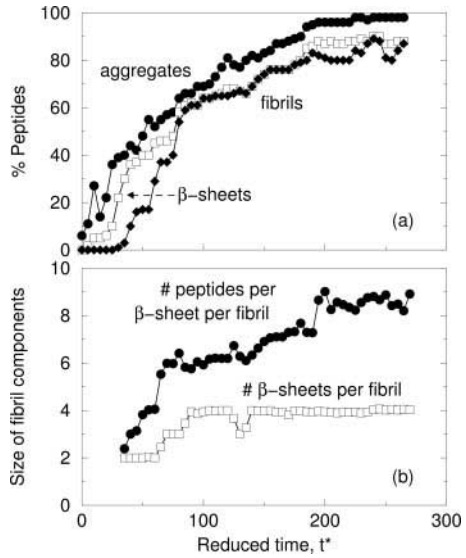

FIG. 3. ***a* and *b*, the percentage of peptides in aggregates (of any type), *β*-sheets, and fibril structures (*a*) and the average number peptides per *β*-sheet in a fibril and the average number of *β*-sheets per fibril (*b*) *versus* reduced time, t^*, for the 48-peptide system at c = 10 mM and T^* = 0.14 (*b*).**

peptide concentration of c = 10 mM. The system was initially equilibrated at a high temperature, T^* = 0.25 and then quickly cooled down to T^* = 0.14 within 0.1 reduced time units. In the snapshots, all hydrophobic side chains are *red*; backbone atoms of different peptides have different colors, assigned so that it will be easy to distinguish the various sheets once the fibril is formed. Starting in random coil conformations at reduced time t^* = 0 (not shown), the chains begin to form small amorphous aggregates almost immediately. These amorphous aggregates have grown by and have collapsed into one big amorphous aggregate by t^* = 12.3. This big amorphous aggregate is not stable and thus disperses by t^* = 19.1 into smaller aggregates, one of which is a three-peptide *β*-sheet (*i.e.* the *purple* *β*-sheet at the *upper right side* of the *box*). Another amorphous aggregate has formed by t^* = 29.0 (*i.e.* at the *upper right side* of the *box*) and released a three-peptide *β*-sheet by t^* = 32.5 (*i.e.* the *dark blue* *β*-sheet in the *lower center* of the *box*). Meanwhile, the *purple* *β*-sheet that was present at t^* = 29.0 has added another peptide, becoming a four-peptide *β*-sheet (*i.e.* at the *right center* of the *box*). Then the system proceeds to form another amorphous aggregate by t^* = 35.3 (*i.e.* at the *upper right section* of the *box*). By t^* = 40.1, this amorphous aggregate has released some of its peptides; the remaining peptides have converted into a small two-sheet structure (the *gray* three-peptide *β*-sheet and the *light blue* two-peptide *β*-sheet at the *right center* of the *box*). Although these two *β*-sheets are at an oblique angle with each other, they eventually realign themselves so that all of their peptides are parallel with one another, creating a small fibrillar aggregate (not shown). In addition, the *purple* *β*-sheet has added more peptides, becoming a six-peptide *β*-sheet by t^* = 40.1 (*i.e.* at the *upper left side* of the *box*). By t^* = 49.0, the *purple* *β*-sheet and the *dark blue* *β*-sheet have approached the small fibrillar structure (*i.e.* at the *right side* of the *box*). However, only the *purple* *β*-sheet is able to attach itself to the fibrillar structure, creating a three-sheet fibrillar structure by t^* = 64.4 (*i.e.* at the *left center* of the *box*). By t^* = 243.0, the *dark blue* *β*-sheet has attached itself to the fibrillar structure, and all of its peptides are parallel with those in the fibrillar aggregate, forming a four-sheet fibril, which itself has grown by adding peptides to the ends of *β*-sheets. The fibrillization process just described exhibits a sequence of events that is typical of many of our simulations at different peptide concentrations and temperatures. In essence, at the beginning of the fibrillization process, the system of denatured peptides stays in a lag phase during which some amorphous aggregates form. These aggregates then convert themselves into small *β*-sheets containing aligned *β*-strands. Once these *β*-sheet structures attain a certain size, they come together and align one by one, creating a small fibril or protofilament. Simultaneously, the fibril grows by adding peptides to the end of each *β*-sheet.

Quantitative analysis of our data confirmed that our simulations exhibited a conformational conversion from amorphous aggregates to small fibrillar structures with subsequent rapid growth of large fibrils. These features were reminiscent of the nucleation steps seen by Serio *et al.* (17) on a yeast prion protein Sup35. They observed fibril formation as a nucleated conformational conversion process in which the formation of small amorphous aggregates containing only 20–80 protein monomers precedes critical nucleus formation. Once nuclei are formed, oligomers, which are initially micelle-like, are added to the fibril end simultaneously. The amorphous aggregates seen in our simulations may be akin to the micelles observed by Soreghan and Glabe (80) during the initial formation of *β*-amyloid fibril; in that case, the micelles were thought to mediate the nucleation events by producing a high local concentration of *β*-amyloid peptides. These conformational conversion features can be seen in Fig. 3, which plots the percentage of peptides in aggregates of all types (amorphous aggregates, fibrils, and non-fibrillar *β*-sheets), *β*-sheets (fibrillar and non-fibrillar) and fibrillar structures, the average number of peptides per *β*-sheet per fibril, and the average number of *β*-sheets per fibril over time t^*. The data here were taken from the simulation at T^* = 0.14 and c = 10 mM shown in Fig. 2. As indicated in Fig. 3*a*, aggregates formed instantaneously. There was a delay time of

20 reduced time units before some of the aggregates converted into a β-sheets and a lag time of 32 reduced time units before fibrils started to appear. As indicated in Fig. 3*b*, the early fibrils were relatively small, containing two β-sheets each consisting of two peptides. The number of β-sheets per fibril increased over time, indicating that the fibril grew in part by adding already formed β-sheets to its side. In addition, the number of peptides per β-sheet increased gradually with time, indicating that the fibril also grew by adding peptides to the end of each β-sheet, thereby lengthening along the fibril axis. Even after the fibril reached its final size of four β-sheets, the number of peptides per β-sheet per fibril continued to increase from 6 to 9 peptides.

We can offer an explanation for the presence of amorphous aggregates, as opposed to ordered aggregates such as β-sheets and small fibrils, both in our model system and in experimental systems, based on an analysis of their energetic properties. For a small ordered aggregate, few residues are completely buried in the core of the structure, so that most of the residues are on the surface. Although the ordered nature of the peptide chains in a β-sheet or fibril yields a dense array of hydrogen bonds and hydrophobic contacts in its core, if the core is small, there are a significant number of exposed hydrophobic side chains and unsatisfied hydrogen bond donors and acceptors on the surface. Amorphous aggregates, on the other hand, tend to contain a web of hydrogen bonds and hydrophobic contacts that is only slightly denser at its center than on its surface. If just a few peptide chains aggregate, an amorphous structure may contain more hydrogen bonds and hydrophobic contacts than an ordered structure and hence be energetically more favorable. As the aggregate size increases, formation of ordered structures is more energetically favorable.

The Rate of Fibril Formation Is a Function of Peptide Concentration and Temperature—Simulations were conducted on unseeded 48-peptide systems initially in a random-coil state at concentrations c = 2.5, 3.75, 5, and 10 mM, which span the range of concentrations at which fibrils can be formed, according to our previous study (56). At each concentration, simulations were performed at constant temperatures of T^* = 0.08, 0.09, 0.10, 0.11, 0.12, 0.13, 0.14, and 0.15, which range from a temperature that is well below the folding temperature for a single α-helix (T^* = 0.11) to a temperature (T^* = 0.15) that is so high that peptides cannot form or maintain hydrogen bonds or hydrophobic interactions, *i.e.* they are in random-coil configurations. The results here are average values from at least 10 simulations at each temperature and concentration. The *error bars* are standard deviations from the average values at each time.

The rate of fibril formation increased with increasing concentration as can be seen in Fig. 4, which plots the percentage of peptides in aggregates of all types (amorphous aggregates, fibrils, and non-fibrillar β-sheets), β-sheets (fibrillar and non-fibrillar), and fibrils as a function of reduced time t^* for the 48-peptide system at a constant temperature of T^* = 0.14 and different peptide concentrations, c = 2.5, 3.75, 5.0, and 10.0 mM. The rates of forming aggregates and β-sheets also increased with increasing concentration. This figure also indicates that the formation of aggregates preceded the formation of β-sheets, which itself preceded the formation of fibrils. In addition, the percentage of peptides in β-sheets was less than the percentage of peptides in aggregates, indicating that not all of the aggregated peptides converted into β-sheets. Likewise, the percentage of peptides in fibrils was less than the percentage of peptides in β-sheets, meaning that not all of the β-sheets became fibrils.

The rate of fibril formation depended on the temperature, as can be seen in Fig. 5, which plots the percentage of peptides in aggregates of all types (amorphous aggregates, fibrils, and non-fibrillar β-sheets), β-sheets (fibrillar and non-fibrillar), and fibrils as a function of time t^* for the 48-peptide system at a constant concentration of c = 10.0 mM and different temperatures, T^* = 0.13, and 0.14. The rate of forming aggregates and β-sheets decreased with increasing temperature. In terms of forming β-sheets, after the system at T^* = 0.13 reached a plateau at ~85%, the system at T^* = 0.14 continued to form more β-sheets, reaching a plateau at 85% by t^* = 200. Although the initial rate of forming fibrils at T^* = 0.13 was greater than that at T^* = 0.14, the rate of fibril formation at T^* = 0.13 later in the simulation was less than that at T^* = 0.14. After the system at T^* = 0.13 reached a plateau at ~40% at t^* = 100, the system at T^* = 0.14 continued to form more fibrils. The reason

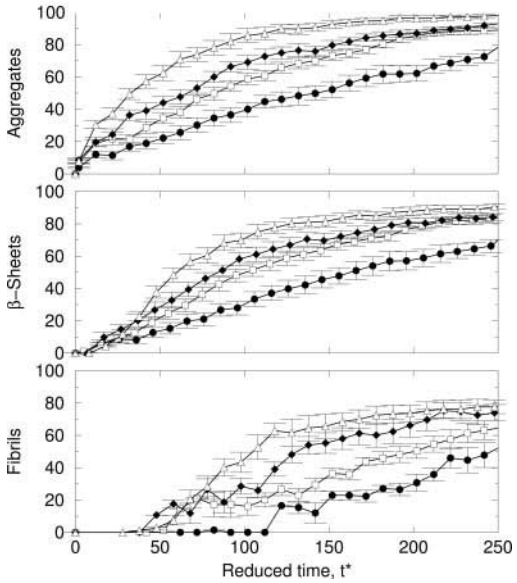

FIG. 4. **The percentage of peptides in aggregates (of any type), β-sheets, and fibril structures *versus* reduced time, t^*, for the 48-peptide system at a constant temperature of T^* = 0.14 and different peptide concentrations c = 2.5 mM (*filled circles*), c = 3.75 mM (*open squares*), c = 5.0 mM (*filled diamonds*), and c = 10.0 mM (*open triangles*).**

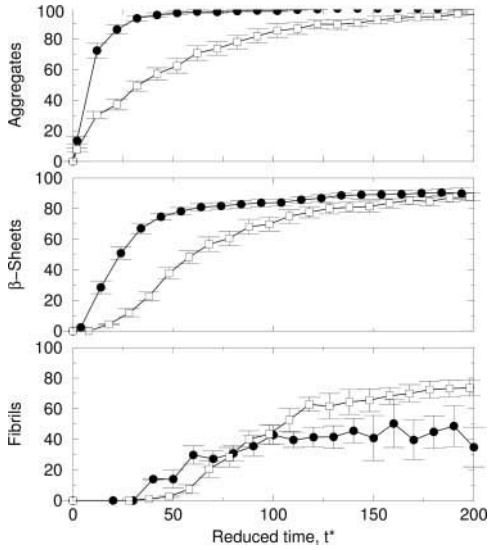

FIG. 5. **The percentage of peptides in aggregates (of any type), β-sheets, and fibril structures *versus* reduced time, t^*, for the 48-peptide system at a constant concentration of c = 10.0 mM and different temperatures T^* = 0.13 (*filled circles*) and T^* = 0.14 (*open squares*).**

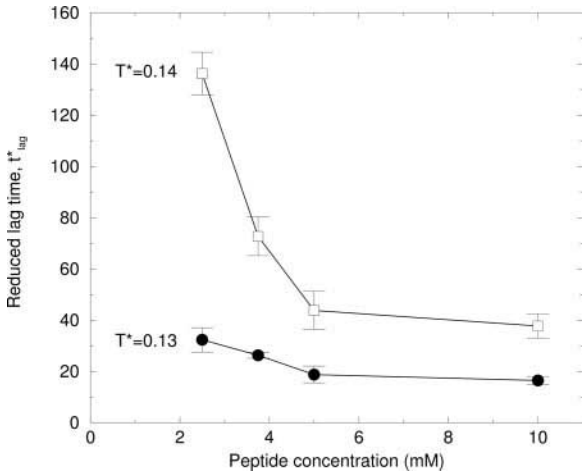

FIG. 6. **The lag time for fibril formation *versus* the concentration for the 48-peptide system at $T^* = 0.13$ and $T^* = 0.14$.**

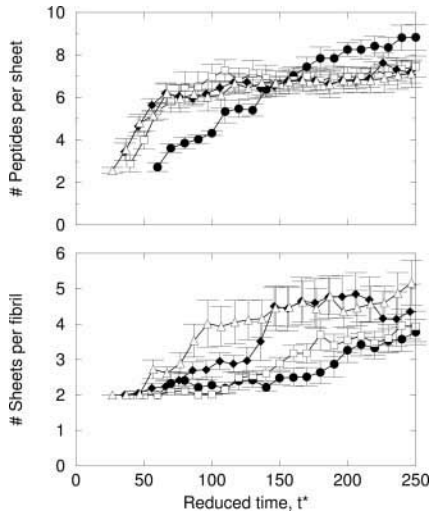

FIG. 7. **The average number of peptides per β-sheet in a fibril and the average number of β-sheets per fibril *versus* reduced time, t^*, for the 48-peptide system at a constant temperature of $T^* = 0.14$ and different peptide concentrations $c = 2.5$ mM (*filled circles*), $c = 3.75$ mM (*open squares*), $c = 5.0$ mM (*filled diamonds*), and $c = 10.0$ mM (*open triangles*).**

that the system at $T^* = 0.13$ stopped growing fibrils after the early stages in the simulation is that it was more likely to be kinetically trapped than the system at $T^* = 0.14$. At $T^* = 0.13$, β-sheets were more likely to collapse onto one another at an oblique angle larger than 35°, thus not satisfying our criteria for classifying an aggregate as a fibril.

Fibril Formation Lag Time as a Function of Peptide Concentration and Temperature—The lag time for the formation of fibrils observed in our simulations decreased with increasing peptide concentration and increased with increasing temperature, as indicated by Fig. 6, which plots the lag time t^* lag *versus* the concentration for the 48-peptide system at $T^* = 0.13$ and $T^* = 0.14$. At $T^* = 0.14$, the lag time decreased exponentially with increasing peptide concentration. However, at $T^* = 0.13$, the decrease in the lag time with peptide concentration did not appear to be an exponential decay; instead, the lag time decreased only slightly with increasing peptide concentration. The rates of decrease in our lag time with peptide concentration were not completely consistent with any of the four proposed mechanisms described in the literature. Although our lag time results at $T^* = 0.14$ were consistent with the nucleated polymerization model, which predicts that $t^*_{\mathrm{lag}} \propto \exp(-c)$, our lag time results at $T^* = 0.13$ were more consistent with the templated assembly model, which predicts that $t^*_{\mathrm{lag}} \approx c$. Interestingly enough, our lag time results at all temperatures were not consistent with the nucleated-conformational conversion model of Serio *et al.* (17), who observed that the lag time is relatively insensitive to the change in peptide concentration; they found, for example, that the lag time over a 500-fold range of concentration decreases by less than 10-fold.

Fibril Growth Proceeds by Both β-Sheet Elongation and Lateral Addition—There were two mechanisms of fibril growth in our simulations: elongation and lateral addition. In β-sheet elongation, the fibril grew by adding individual peptides to the end of each β-sheet. In lateral addition, the fibril grew by adding already formed β-sheets to its side. Both mechanisms can be seen in the snapshots in Fig. 2 and in the data for $c = 10$ mM and $T^* = 0.14$ on the average number of peptides per β-sheet in a fibril and the average number of β-sheets per fibril in Fig. 3*b*. These two growth mechanisms were observed in all of our simulations at different conditions as illustrated in Fig. 7, which plots the average number of peptides per β-sheet in a fibril and the average number of β-sheets per fibril *versus* reduced time, t^*, for the 48-peptide system at a constant temperature of $T^* = 0.14$ and different peptide concentrations, $c = 2.5$, 3.75, 5.0, and 10.0 mM. Each data point is an average value from at least 10 simulations. Fig. 7 shows that there was a more or less gradual increase in the average number of peptides per β-sheet in a fibril as a function of time, increasing from two to nine peptides per β-sheet in a fibril. Fig. 7 also shows that there was a gradual increase in the average number of β-sheets per fibril as a function of time, increasing from two to five β-sheets per fibril. Toward the end of each simulation, the fibrils contained between three and five β-sheets, each with six to nine peptides. This was also observed in our previous simulation study (56) of the slow-cooling formation of fibrils in systems containing 12–96 peptides at $c = 5$ mM, $R = 1/10$, and $T^* = 0.13$.

Once the fibrillar structure reached its critical β-sheet number, monomeric peptides tended to attach to it rather than creating an isolated β-sheet. These two growth mechanisms were similar to those observed in experiments by Green *et al.* (81), who found two distinct phases in human amylin fibrillogenesis in which lateral growth of oligomers was followed by longitudinal growth into mature fibrils. There is an energetic explanation for the tendency of the fibrils to grow very long along the fibril axis rather than to grow laterally by including more and more β-sheets. We can imagine growth of the complex as occurring either by the addition of a peptide that extends a sheet or by the addition of a peptide that creates a new sheet. This is illustrated in Fig. 8, which shows the numbers of HB and HP between an inner peptide, labeled *P*, and the adjacent peptides in the structure. Positions A and B represent possible extensions of the fibril core. A peptide in position A, which represents β-sheet elongation, would form 15 hydrogen bonds and 27 hydrophobic interactions (14 intrasheet and 13 intersheet) with the existing fibril scaffold, whereas a peptide at position B, which represents β-sheet creation, would form only 26 hydrophobic interactions. Therefore, there is an energetic preference for β-sheet elongation (position A) as opposed to β-sheet creation (position B). This energetic preference would help to explain the asymmetric fibril growth that is seen in nature, where fibrils are composed of four to six β-sheets and each β-sheet is made up of hundreds or thousands of protein chains (74, 77–79).

Fibril Formation Is Nucleation-dependent—Fibril formation involved a nucleation event, as suggested by our seeded simulations in which previously created fibrils were immersed in a sea of denatured chains. The results from these seeded simu-

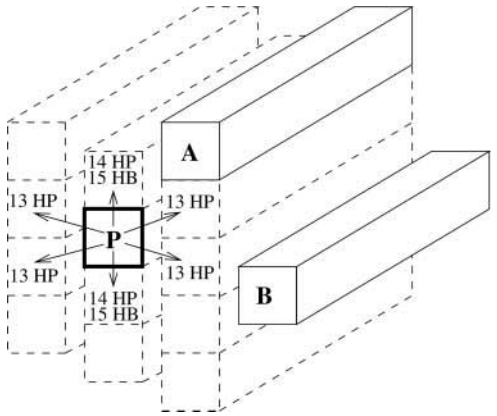

FIG. 8. **Schematic showing peptide locations within the fibril indicating the types of interactions (HP or HB) between an inner peptide, labeled *P*, and the adjacent peptides in the structure.** *Positions A* and *B* represent possible extensions of the core of the fibril.

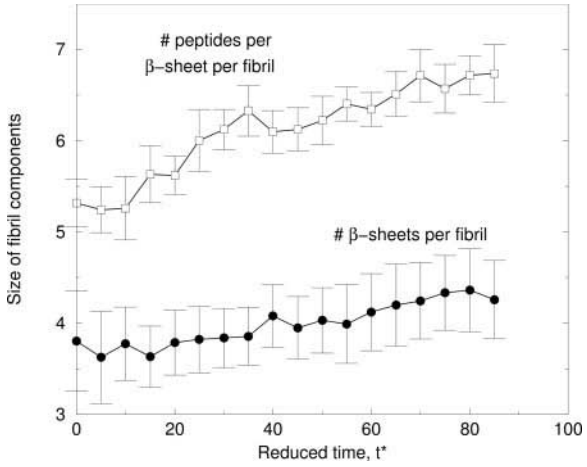

FIG. 9. **The average number of peptides per sheet in a fibril and the average number of β-sheets per fibril *versus* reduced time, *t**, from the seeded simulations of the 96-peptide system at *c* = 2.0 mM and *T** = 0.15.**

lations at $T^* = 0.15$ are shown in Fig. 9, which plots the average number of peptides per β-sheet per fibril and the average number of β-sheets per fibril over time t^*. This figure indicates that the average number of β-sheets per fibril remained constant at four, whereas the average number of peptides per β-sheet per fibril increased from approximately five to almost seven over time. This was consistent with data (not shown) indicating that there were no new fibrils formed in the system. Denatured random-coil peptides formed fibrils not by creating new ones but by attaching themselves onto the seeded fibril. In other words, the seeded fibril grew at $T^* = 0.15$ by adding monomeric denatured peptides to the ends of its β-sheets. This is in contrast to the constant temperature unseeded simulation results presented here and the results from our previous slow-cooling unseeded simulation study (56) in which fibril formation occured only at temperatures up to $T^* = 0.14$. In all unseeded simulations, the kinetic energy was too high at $T^* = 0.15$ to form and maintain any hydrogen bonds or hydrophobic interactions; therefore, peptides at all concentrations considered were random coils (data not shown). Comparison of the results from seeded and unseeded simulations at $T^* = 0.15$ suggests that fibril formation is a nucleation-dependent process, which is similarly observed in various experimental studies (3, 17, 75, 82).

Fibril formation in our simulations could bypass the slow

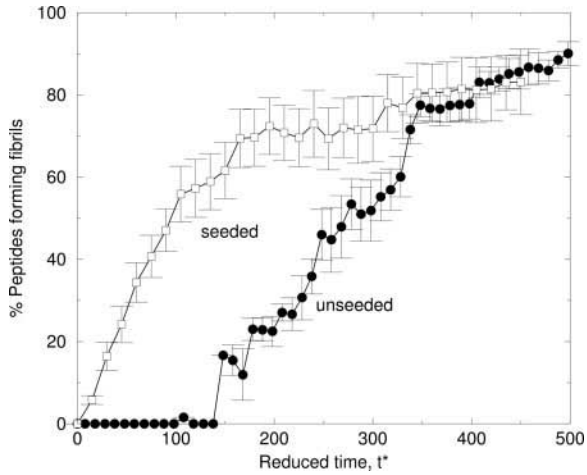

FIG. 10. **The percentage of peptides in fibril structures *versus* reduced time, *t**, from the seeded and unseeded simulations of systems at *c* = 2.0 mM and *T** = 0.14.**

nucleation step in the presence of preformed nucleus or seed. This is shown in Fig. 10, which plots the percentage of the 48 random-coil peptides inserted into the seeded systems that attach to the fibrils (resulting in fibril growth) as a function of the reduced time, t^*, at $c = 2.0$ mM and $T^* = 0.14$. The percentages of peptides that are in fibrils during the unseeded simulations at the same condition is also plotted for comparison. The lag time for fibril formation from the unseeded simulations was about 135 reduced time units as compared with a lag time of zero for fibril formation in the unseeded simulations. This indicates that in the presence of a nucleus, random coils readily attached to the fibrils without going through the nucleation step after a long lag time.

Conclusions—Computer simulations offer unique opportunities to observe and analyze molecular level events in fibril formation that are difficult or impossible to observe experimentally. In simulating large multipeptide systems using our intermediate resolution protein model, PRIME, in conjunction with the discontinuous molecular dynamics, we have been able to examine the kinetics of the fibrillization process of polyalanines to discern the molecular level mechanisms responsible for nucleation and fibril growth at a variety of conditions. Two types of simulations were conducted: unseeded simulations and seeded simulations.

In unseeded simulations, the initial systems contained random-coil peptides. In the seeded simulations, already formed fibrils were immersed in a sea of denatured peptides. The ability of a system to form fibrils at high temperatures depended upon whether there was a seeded structure present in the system. In the unseeded simulations, fibril formation occurred only at temperatures up to $T^* = 0.14$; at $T^* = 0.15$ and higher temperatures, peptides at all concentrations considered were random coils. However, in the seeded simulations at $T^* = 0.15$, random-coil peptides attached themselves to the seeded fibrils, indicating that in the presence of seeds or nuclei, fibrils could form at even higher temperature. At $T^* = 0.14$, fibril formation occurred quickly in the presence of nucleus as compared with the long lag times that were seen in the unseeded simulations at the same temperatures. These results indicate that fibril formation was nucleation-dependent, which is similarly observed in experiments (3, 17, 75, 82).

In the unseeded simulations, there was a lag time before fibril formation commenced; the lag time depended upon the temperature and peptide concentration. At high temperatures, the lag time decreased more or less exponentially as a function of concentration, as suggested by the nucleated polymerization

model (14–16). At low temperatures, the lag time decreased more or less linearly with increasing peptide concentration as suggested by the templated assembly model (11, 12). In addition, fibril formation was preceded by the appearance of amorphous aggregates and then β-sheets, which is similar to the features of the nucleated conformational conversion model proposed by Serio *et al.* (17) on yeast prion proteins and the initial micelle formation steps observed by Soreghan and Glabe (80) on β-amyloid peptides. Unlike the nucleated conformational conversion model in which fibril growth is through the addition of globular multimers to fibril ends, fibril growth in our simulations involved both β-sheet elongation, in which the fibril grew by adding individual peptides to the end of each β-sheet, and lateral addition, in which the fibril grew by adding already formed β-sheets to its side. Finally, the rate of fibril formation depended upon the temperature and peptide concentration; specifically, the initial rate of fibril formation increased with increasing concentration and decreased with increasing temperatures. Despite the similarities between selected features observed in our simulations and the behavior predicted by the templated assembly, nucleated polymerization, and nucleated conformational conversion models, none of these gives a fully satisfactory description of the simulation kinetics of fibril formation by polyalanine peptides.

Acknowledgments—We are grateful to Sylvie Blondelle, Ken Dill, Jeffery Kelly, and Dan Kirschner for helpful discussions.

REFERENCES

1. Kirschner, D. A., Abraham, C, and Selkoe, D. J. (1986) *Proc. Natl. Acad. Sci. U. S. A.* **83,** 503–507
2. Kelly, J. W. (1998) *Curr. Opin. Struct. Biol.* **8,** 101–106
3. Koo, E. H., Lansbury, P. T., Jr., and Kelly, J. W. (1999) *Proc. Natl. Acad. Sci. U. S. A.* **96,** 9989–9990
4. Selkoe, D. J. (1999) *Nature* **399,** A23–A31
5. Lynn, D. G., and Meredith, S. C. (2000) *J. Struct. Biol.* **130,** 153–173
6. Conway, K. A., Lee, S. J., Rochet, J. C., Ding, T. T., Williamson, R. E., and Lansbury, P. T., Jr. (2000) *Proc. Natl. Acad. Sci. U. S. A.* **97,** 571–576
7. Guijarro, J. I., Sunde, M, Jones, J. A., Campbell, I. D., and Dobson, C. M. (1998) *Proc. Natl. Acad. Sci. U. S. A.* **95,** 4224–4228
8. Chiti, F., Webster, P., Toddei, N., Clark, A., Stefan, M., Ramponi, G., and Dobson, C. M. (1999) *Proc. Natl. Acad. Sci. U. S. A.* **96,** 3590–3594
9. Chiti, F., Bucciantini, M., Capanni, C., Taddei, N., Dobson, C. M., and Stefan, M. (2001) *Protein Sci.* **10,** 2541–2547
10. Kelly, J. W. (2000) *Nat. Struct. Biol.* **7,** 824–826
11. Uratani, Y., Asakura, S., and Imahori, K. (1972) *J. Mol. Biol.* **67,** 85–98
12. Griffith, J. S. (1967) *Nature* **215,** 1043–1044
13. Prusiner, S. B. (1982) *Science* **216,** 136–144
14. Jarrett, J. T., and Lansbury, P. T. (1993) *Cell* **73,** 1055–1058
15. Hofrichter, J., Ross, P. D., and Eaton, W. (1974) *Proc. Natl. Acad. Sci. U. S. A.* **71,** 4864–4868
16. Beaven, G. H., Gratzer, W. B., and Davies, H. G. (1969) *Eur. J. Biochem.* **11,** 37–42
17. Serio, T. R., Cashikar, A. G., Kowal, A. S., Sawicki, G. J., Moslehi, J. J., Serpell, L., Arnsdorf, M. F., and Lindquist, S. L. (2000) *Science* **289,** 1317–1321
18. Kortvelyesi, T., Kiss, G., Murphy, R. F., Penke, B., and Lovas, S. (2001) *J. Mol. Structure* **545,** 215–223
19. Straub, J. E., Guevara, J., Huo, S, and Lee, J. P. (2002) *Acc. Chem. Res.* **35,** 473–481
20. Massi, F., Peng, J. W., Lee, J. P., and Straub, J. E. (2001) *Biophys. J.* **81,** 31–44
21. Massi, F., Klimov, D., Thirumalai, D., and Straub, J. E. (2002) *Protein Sci.* **11,** 1639–1647
22. Massi, F., and Straub, J. E. (2001) *J. Comput. Chem.* **24,** 143–153
23. Massi, F., and Straub, J. E. (2001) *Biophys. J.* **81,** 697–709
24. Moraitakis, G., and Goodfellow, J. M. (2003) *Biophys. J.* **84,** 2149–2158
25. Ilangovan, U., and Ramamoorthy, A. (1998) *Biopolymers* **45,** 9–20
26. Yang, M., Lei, M., and Huo, S. (2003) *Protein Sci.* **12,** 1222–1231
27. Li, L., Darden, T. A., Bartolotti, L., Kominos, D., and Pedersen, L. G. (1999) *Biophys. J.* **76,** 2871–2878
28. George, A. R., and Howlett, D. R. (1999) *Biopolymers* **50,** 733–741
29. Ma, B., and Nussinov, R. (2002) *Protein Sci.* **11,** 2335–2350
30. Ma, B., and Nussinov, R. (2002) *Proc. Natl. Acad. Sci. U. S. A.* **99,** 14126–14131
31. Zanuy, D., Ma, B., and Nussinov, R. (2003) *Biophys. J.* **84,** 1884–1894
32. Zanuy, D., and Nussinov, R. (2003) *J. Mol. Biol.* **329,** 565–584
33. Lakdawala, A. S., Morgan, D. M., Liotta, D. C., Lynn, D. G., and Snyder, J. P. (2002) *J. Am. Chem. Soc.* **124,** 15150–15151
34. Hwang, W., Marini, D. M., Kamm, R. D., and Zhang, S. (2003) *J. Chem. Phys.* **118,** 389–397
35. Kuwata, K., Matumoto, T., Cheng, H., Nagayama, K., James, T. L., and Roder, H. (2003) *Proc. Natl. Acad. Sci. U. S. A.* **100,** 4790–4795
36. Gsponer, J., Haberthur, U., and Caflisch, A. (2003) *Proc. Natl. Acad. Sci. U. S. A.* **100,** 5154–5159
37. Mager, P. P. (1998) *Molecular Simulation* **20,** 201–222
38. Mager, P. P. (1998) *Med. Res. Rev.* **18,** 403–430
39. Mager, P. P., Reinhardt, R., and Fischer, K. (2001) *Molecular Simulation* **26,** 367–379
40. Fernandez, A., and Boland, Mde. L. (2002) *FEBS Lett.* **529,** 298–302
41. Klimov, D. K., and Thirumalai, D. (2003) *Structure* (*Camb.*) **11,** 295–307
42. Jang, H., Hall, C. K., and Zhou, Y. (2004) *Biophys. J.* **86,** 31–49
43. Jang, H., Hall, C. K., and Zhou, Y. (2004) *Protein Sci.* **13,** 40–53
44. Ding, F., Dokholyan, N. V., Buldyrev, S. V., Stanley, H. E., and Shakhnovich, E. I. (2002) *J. Mol. Biol.* **324,** 851–857
45. Sun, S. (1993) *Protein Sci.* **2,** 762–785
46. Sun, S., Thomas, P. D., Dill, K. A. (1995) *Protein. Eng.* **8,** 769–778
47. Takada, S., Luthey-Schulten, Z., and Wolynes, P. G. (1999). *J. Chem. Phys.* **110,** 11616–11629
48. Smith, A. V., and Hall, C. K. (2001) *Proteins Struct. Funct. Genet.* **44,** 344–360
49. Nguyen, H. D., Marchut, A. J., and Hall, C. K. (2004) *Protein Sci.***13,** 2909–2924
50. Smith, A. V., and Hall, C. K. (2001) *Proteins Struct. Funct. Genet.* **44,** 376–391
51. Smith, A. V., and Hall, C. K. (2001) *J. Mol. Biol.* **312,** 187–202
52. Alder, B. J., and Wainwright, T. E. (1959) *J. Chem. Phys.* **31,** 459–466
53. Rapaport, D. C. (1978) *J. Phys. A: Math. Gen.* **11,** L213–L217
54. Rapaport, D. C. (1979) *J. Chem. Phys.* **71,** 3299–3303
55. Bellemans, A., Orban, J., and VanBelle, D. (1980) *Mol. Phys.* **39,** 781–782
56. Nguyen, H. D, and Hall, C. K. (2004) *Proc. Natl. Acad. Sci. U. S. A.* **101,** 16180–16185
57. Andersen, H. C. (1980) *J. Chem. Phys.* **72,** 2384–2393
58. Brais, B., Rouleau, G. A., Bouchard, J. P., Farde, M., and Tome, F. M. S. (1999) *Semin. Neurol.* **19,** 59–66
59. Forood, B., Perez-Paya, E., Houghten, R. A., and Blondelle, S. E. (1995) *Biochem. Biophys. Res. Commun.* **211,** 7–13
60. Blondelle, S. E., Forood, B., Houghten, R. A., and Perez-Paya, E. (1997) *Biochemistry* **36,** 8393–8400
61. Simmons, L., May, P., Tomaselli, K., Rydel, R., Fuson, K., Brigham, E., Wright, S., Lieberburg, I., Becker, G., Brems, D., and Li, W. (1994) *Mol. Pharmacol.* **45,** 373–379
62. Horwich, A. L., and Weissman, J. S. (1997) *Cell* **89,** 499–510
63. Sunde, M., and Blake, C. (1997) *Adv. Protein Chem.* **50,** 123–159
64. Kusumoto, Y., Lomakin, A., Teplow, D. B., and Benedek, G. B. (1998) *Proc. Natl. Acad. Sci. U. S. A.* **95,** 12277–12282
65. Harrison, P. M., Chan, H. S., Prusiner, S. B., and Cohen, F. E. (1999) *J. Mol. Biol.* **286,** 593–606
66. Esler, W. P., Felix, A. M., Stimson, E. R., Lachenmann, M. J., Ghilardi, J. R., Lu, Y. A., Vinters, H. V., Mantyh, P. W., Lee, J. P., and Maggio, J. E. (2000) *J. Struct. Biol.* **130,** 174–183
67. Ding, F., Borreguero, J. M., Buldyrey, S. V., Stanley, H. E., and Dokholyan, N. V. (2003) *Proteins Struct. Funct. Genet.* **53,** 220–228
68. Irback, A., Sjunnesson, F., and Wallin, S. (2000) *Proc. Natl. Acad. Sci. U. S. A.* **97,** 13614–13618
69. Smith, S. W., Hall, C. K., and Freeman, B. D. (1997) *J. Comp. Phys.* **134,** 16–30
70. Zhou, Y., Karplus, M., Wichert, J. M., and Hall, C. K. (1997) *J. Chem. Phys.* **107,** 10691–10708
71. Benzinger, T. L., Gregory, D. M., Burkoth, T. S., Miller-Auer, H., Lynn, D. G., Botto, R. E., and Meredith, S. C. (1998) *Proc. Natl. Acad. Sci. U. S. A.* **95,** 13407–13412
72. Antzutkin, O. N., Balbach, J. J., Leapman, R. D., Rizzo, N. W., Reed, J., and Tycko, R. (2000) *Proc. Natl. Acad. Sci. U. S. A.* **97,** 13045–13050
73. Balbach, J., Petkova, A., Oyler, N., Antzutkin, O., Gordon, D., Meredith, S., and Tycko, R. (2002) *Biophys. J.* **83,** 1205–1216
74. Sunde, M, Serpell, L. C., Bartlam, M, Fraser, P. E., Pepys, M. B., and Blake, C. C. F. (1997) *J. Mol. Biol.* **273,** 729–739
75. Harper, J. D., Lieber, C. M., and Lansbury, P. T., Jr. (1997) *Chem. Biol.* **4,** 951–959
76. Jarvis, J., Craik, D., and Wilce, M. (1993) *Biochem. Biophys. Res. Commun.* **192,** 991–998
77. Serpell, L. C., Sunde, M., Benson, M. D., Tennent, G. A., Pepys, M. B., and Fraser, P. E. (2000) *J. Mol. Biol.* **300,** 1033–1039
78. Malinchik, S. B., Inouye, H., Szumowski, K. E., and Kirschner, D. A. (1998) *Biophys. J.* **74,** 537–545
79. Burkoth, T. S., Benzinger, T. L. S., Urban, V, Morgan, D. M., Gregory, D. M., Thiyagarajan, P., Botto, R. E., Meredith, S. C., and Lynn, D. G. (2000) *J. Am. Chem. Soc.* **122,** 7883–7889
80. Soreghan, B., and Glabe, J. K. C. (1994) *J. Biol. Chem.* **269,** 28551–28554
81. Green, J. D., Goldsbury, C, Kistler, J., Cooper, G. S., and Aebi, U. (2004) *J. Biol. Chem.* **279,** 12206–12212
82. Wilkins, D. K., Dobson, C. M., and Gross, M. (2000) *Eur. J. Biochem.* **267,** 2609–2616